Inertial capillary uptake of drops

Geoff R. Willmott*
Department of Physics and School of Chemical Sciences, The University of Auckland, Auckland, New Zealand, and The MacDiarmid Institute for Advanced Materials and Nanotechnology, Wellington, New Zealand

Alice Briole† and Florence Szczepaniak‡
Départements Physique et Chimie, École normale supérieure de Lyon, 69342 Lyon, France

(Received 21 January 2019; revised manuscript received 25 July 2019; accepted 25 March 2020; published 24 April 2020)

Uptake of liquid drops into capillary tubes has been experimentally studied and quantitatively analyzed. In experiments, drops of water and aqueous glycerol ($\leqslant$50 wt %) were drawn into cylindrical borosilicate glass and quartz tubes with an inner diameter of 0.50–0.75 mm. The meniscus height rise was measured using high-speed images captured at 4000 frames per second, and results within a conservatively defined inertial regime indicate constant uptake velocity. An increase in the inertial velocity with drop curvature was observed due to increasing Laplace pressure in the drop, as drop sizes were comparable to the width of the capillary tubes. Measured velocities were slower than predicted by a purely inertial-capillary model and best described by introducing a contact line friction, consistent with the observed variability and viscosity dependence of the results. Mean friction coefficients in borosilicate capillaries ranged from 169 ± 1 for 50 wt % glycerol drops to 218 ± 1 for water drops. Peaks in the instantaneous Laplace pressure caused by surface oscillations were also measured. Correlations with uptake velocity were qualitatively apparent, with a delay between peaks of similar magnitude to the inertial-capillary oscillation time.

DOI: 10.1103/PhysRevE.101.043109

I. INTRODUCTION

Capillary uptake of droplets is of wide importance in nature, industry, and everyday life. The general phenomenon has been widely studied, and a wealth of previous experimental work has been reviewed [1–5]. Nevertheless, various aspects of capillarity continue to challenge our understanding. This paper is particularly concerned with the dynamics involved in capillary uptake of drops, when the drop diameter is of comparable size to the tube opening. This situation is important for drops in confined spaces, such as during irrigation, drop uptake into porous materials [6,7], and catalytic growth of carbon nanotubes [8,9]. Controlled manipulation of drops using structures like capillary valves [10] has become an important topic in microfluidics, and there are also potential macroscopic applications in low gravity [2].

Analytic models for capillary uptake of an incompressible, Newtonian liquid in air have evolved from studies of uptake into a vertical cylindrical tube of radius r_t from a reservoir [Fig. 1(a)]. The main concern is the height of the meniscus h as a function of time t. Summaries of work on this problem were given by Stange *et al.* [2] and Kornev and Neimark [11], who included factors such as liquid inertia, the pressure drop in and below the tube entrance [12,13], and initial development of the meniscus. Building on those models, some previous capillary uptake studies [3,6,9,14,15] have considered uptake from a droplet [Figs. 1(b)–1(d)]. A spherical drop produces a Laplace pressure external to the capillary given by $\Delta P = 2\gamma/R$, where γ is the fluid's surface tension in air and R is the drop radius. The dynamics can also be affected by friction at the three-phase contact line inside the tube [4], described by the coefficient χ.

A differential equation for the height of the meniscus may be obtained by considering the momentum of flow into the capillary (see the Supplemental Material [16] for further details),

$$\rho\frac{d^2h}{dt^2}(h+cr_t)+\rho\kappa\left(\frac{dh}{dt}\right)^2+\frac{2\chi\eta}{r_t}\frac{dh}{dt}+\frac{8\eta}{r_t^2}h\frac{dh}{dt}+\rho gh = 2\gamma\left(\frac{s\cos\theta}{r_t}+\frac{1}{R}\right). \quad (1)$$

where ρ and η are the fluid's density and viscosity, respectively, g is gravitational acceleration, θ is the contact angle of the liquid with the tube, and c, κ, and s are parameters discussed below. From left to right, the first two terms can be identified with inertia, and the next represents friction. The fourth term represents viscosity, the fifth represents gravity, and the driving capillary force is on the right-hand side of the equation. Many aspects of capillary uptake can be explained by applying simplifying assumptions to Eq. (1). For example, the famous Lucas-Washburn equation [5,17,18] which yields $h \propto t^{\frac{1}{2}}$ dependence is obtained when $R^{-1} = 0$ and viscous

*Corresponding author: g.willmott@auckland.ac.nz
†alice.briole@ens-lyon.fr
‡florence.szczepaniak@ens-lyon.fr

 ©2020 American Physical Society

effects dominate inertia and gravity, so that all terms other than the fourth and sixth are neglected.

In this study of drop uptake dynamics, high-speed photography is used to measure the advance of the meniscus as a function of time in single cylindrical glass capillaries. The external fluid is composed of water and aqueous glycerol drops placed on a superhydrophobic surface. Our data are used to explore aspects of Eq. (1) by following two relevant research directions. The first is uptake in which the drop produces significant Laplace pressure external to the capillary tube ($R^{-1} \neq 0$). The curvature of drops in our experiments is comparable to the meniscus curvature within the tube. The second research direction is the study of the so-called inertial (or "inviscid") regime, where h is small (particularly relevant for small drops) and the viscous term is not important.

Previous experimental studies of droplet capillary uptake have shown that drops (in contrast to reservoirs) can penetrate a nonwetting capillary or pore, can affect the speed of uptake, and can determine the direction of meniscus motion in a prefilled capillary [3,7,15,19–21]. Experimental configurations have involved nonwetting capillaries ($\theta > 90^\circ$, [3,19,20,22]), fluids with viscosity greater than water [20,21], and drops with an initial velocity [22]. Aside from experiments, drop uptake has been studied computationally [8,9,23,24]. Other studies of modifications to external Laplace pressure in capillary uptake have included Laplace pressures caused by finite container size [2] or the meniscus on the outside of the capillary [4].

A quantitative description of drop uptake dynamics has not been established in these previous works. Variation in the process by which the tube and drop come into contact is one complicating factor [19]. Another is the reduction of the size of the drop outside the tube over time, so that both the Laplace pressure and its rate of change increase as the drop becomes smaller. In previous work, authors have sometimes relied on well-known Lucas-Washburn dynamics, whereas uptake of drops can take place predominantly in the inertial regime. In contrast, uptake regimes defined for reservoirs (including the inertial regime) are reasonably well described by steady-state forces.

Studies of the inertial regime have become more common in recent decades due to the increased availability of high-speed photography. For uptake from reservoirs, good explanations of this regime are available [1,2,25–27], and recent progress has included studies of inertial uptake into a short capillary [28] and porous networks [29]. A key analytical development [25] was identification of a linear regime ($h \propto t$) from the inertial (second) and capillary (sixth) terms in Eq. (1) for the case $\kappa = 1$, $R^{-1} = 0$, yielding the velocity $v_B = (2\gamma \cos\theta/\rho r_t)^{\frac{1}{2}}$. This is sometimes referred to as the Bosanquet velocity.

Experiments in the inertial regime typically produce linear uptake ($h \propto t$), but measured velocities are consistently smaller than v_B [1,4,20,25]. Low experimental velocities have been explained using an increased effective viscosity [5,26], and it should be noted from Eq. (1) that v_B is lowered when $c > 0$ or $\kappa > 1$. The parameter c accounts for inertia of the flow below the tube entrance, taking a value of order 1 [2,11]. However, the first term in Eq. (1) may be neglected if h and the acceleration are small, which is assumed in the derivation of v_B. The parameter κ accounts for excess pressure drop due to development of the velocity profile near the entrance and takes a value close to 7/6 [2], which suggests a 7% reduction in v_B.

In previous work, explanations for experimental velocities lower than v_B have commonly involved the contact angle. From a typical starting assumption of $\theta = 0^\circ$, lower velocities can be explained by a dynamic contact angle (DCA) which increases with meniscus velocity. The DCA has been especially well studied in the Lucas-Washburn regime, and various DCA models have been used [5,21,26,30–32] and explicitly compared [33,34] in capillarity uptake experiments. However, in a recent study of the inertial regime using a high-resolution x-ray technique, Andrukh *et al.* [4] found that the DCA did not vary greatly from the equilibrium angle. A better explanation for their results was obtained using contact line friction, included as the third term in Eq. (1). χ should be a material property at the three-phase contact line and is independent of r_t. Friction is expected to arise from the forces required to move a contact line over a real surface with stochastic pinning points [35]. Even on an ideal surface, analytic models require a precursor film to alleviate a singularity at the contact line, and there is a contribution to friction from disjoining pressures associated with this film [4].

Theoretical development

For our study of drop uptake in the inertial regime, we modify Eq. (1) as follows. Following the same method used to derive v_B [26], the first term containing accelerations is neglected for short timescales consistent with the inertial regime. This omission is supported by the experimental data (see Sec. III B) which show that the meniscus does not strongly accelerate within this regime. The fourth (viscous) term is removed on the basis that the data analyzed are within the inertial regime, which will be discussed and further justified in Sec. III B. For these early stages of uptake, the liquid surface area in contact with the capillary wall is small, so viscous drag is small even though friction generated by the contact line (which has constant length) can be large. Thus, in our experiments, the ratio of the fourth to third terms in Eq. (1) (using v_B and r_t as velocity and length scales, respectively) does not exceed 0.05 for typical scaling of $\chi \sim 100$ [4]. Gravity can usually be neglected for millimetric drops, as the capillary length for water in air is 2.7 mm. The Bond number (equal to $\rho g r_t/\gamma$) does not exceed 0.025 in our experiments. The parameter s accounts for initial development of the meniscus [2], and here, we set $s = 1$, which is accurate to within 0.3% for our data after 0.5 ms (corresponding to two photographic frames). Therefore,

$$\rho\kappa\left(\frac{dh}{dt}\right)^2 + \frac{2\chi\eta}{r_t}\frac{dh}{dt} = 2\gamma\left(\frac{\cos\theta}{r_t} + \frac{1}{R}\right), \tag{2}$$

and we use the value $\kappa = 7/6$ in calculations (see above). Velocities for special cases can be identified using Eq. (2). The first, equivalent to v_B but for drop uptake, is the linear inertial velocity when the friction term is ignored,

$$v_{B,R} = \left[\frac{2\gamma}{\kappa\rho}\left(\frac{\cos\theta}{r_t} + \frac{1}{R}\right)\right]^{\frac{1}{2}}. \tag{3}$$

To obtain Eq. (3), it has been assumed that R is not time dependent.

TABLE I. Material properties and selected calculations for the solutions used in experiments. Velocities are calculated using Eq. (3) for 0.75-mm tubes unless otherwise indicated.

	Density	Viscosity	Surface tension	$v_{B,R}$		
Solution	ρ (kg m^{-3})	η (mPa s)	γ (mJ m^{-2})	Reservoir (mm s^{-1})	$R_0 = 1$ mm (mm s^{-1})	$t_2/4$ (ms)
Water	998	1.01	72.8	577	677	34.9
0.50 mm				707	791	15.5
Glycerol						
10 wt %	1022	1.30	71	564	661	27.7
30 wt %	1073	2.46	70	546	641	15.4
50 wt %	1126	6.00	67	522	612	65.2

When including friction, it is possible to obtain a velocity which neglects inertia entirely. Here, we add the drop Laplace pressure to Andrukh *et al.*'s value for reservoir uptake [4], obtaining

$$v_{f,R} = \frac{\gamma}{\chi\eta}\left(\cos\theta + \frac{r_t}{R}\right). \tag{4}$$

If inertia and friction are both important, all terms in Eq. (2) can be used to obtain a quadratic equation for dh/dt. The positive-velocity solution is

$$v_{B,f,R} = \frac{\left[\eta^2\chi^2 + 2\kappa\rho r_t\gamma\left(\cos\theta + \frac{r_t}{R}\right)\right]^{\frac{1}{2}} - \eta\chi}{\kappa\rho r_t}. \tag{5}$$

Equation (5) can be obtained from Eq. (2) without integration, so it has not been assumed that R is constant.

Below, we initially describe and present our experimental results, then analyze them according to the analytical frameworks described above. In the latter part of the paper, we use an image analysis method for measuring the instantaneous curvature of the drop outside of the tube in order to explore details of the uptake dynamics.

II. MATERIALS AND METHODS

A. Experimental details

Deionized (Milli-Q) water and aqueous glycerol (Sigma-Aldrich) solutions were used, with material properties as in Table I. Density ρ and viscosity η were obtained from literature values at 20 °C [36], as was the surface tension in air γ for water [37]. For glucose solutions, γ was determined using the pendant drop method, in which the shape of an axisymmetric drop hanging from a capillary tube in mechanical equilibrium is analyzed [Fig. 2(a)] and compared with theory [38]. Uncertainties in this measurement (± 1 mJ m^{-2}) and other material properties are considered to be less significant than stochastic variations in the data obtained below.

The three types of capillary tube used in experiments were borosilicate glass tubes with an inner diameter (i.d.) of 0.75 mm and outer diameter (o.d.) of 1 mm, borosilicate glass tubes with i.d. of 0.50 mm and o.d. of 1 mm, and quartz tubes with i.d. of 0.50 mm and o.d. of 1 mm (all from Sutter Instruments). Diameters are nominal values provided by the manufacturer, and tubes are referred to by their inner diameters elsewhere in this paper. Capillaries were either used as received or cleaned by immersing them in a solution of water, ammonium, and hydrogen peroxide (5:1:1) at 70 °C for 20 min, then rinsing with water and isopropanol, and finally drying with nitrogen gas. For the experiment in Fig. 6(a) below, the capillary was cleaned by boiling in a solution of water and acetone at 70 °C for 20–30 min and using an ultrasonic cleaner. Once the solution cooled down, the tube was rinsed with cold deionized water and absolute ethanol and dried in a stream of nitrogen.

Superhydrophobic surfaces were made by electroless deposition of silver on to copper plates followed by thiolation, using a well-established procedure [39], or else by application of Ultra-Ever Dry (UltraTech International) to clean glass slides. Droplets on either type of surface have typical contact angles of 160°–175°. Drops were dispensed on to the superhydrophobic surfaces using an uncontrolled spray from a fine needle tip. This produced a range of droplet sizes and contact angles, as drops are preferentially immobilized at surface impurities. A drop with a relatively high curvature (and therefore contact angle, typically >160°) was selected, and the capillary was aligned vertically above the drop. As the capillary was slowly lowered into contact using a threaded mount, so that the velocity at contact was typically <1 mm s^{-1}, a high-speed sequence was recorded. Two high-speed cameras (Photron Fastcam SA5 and AX50, BlinkTech, Australia) were set up to record capillary uptake events, with horizontal lines of sight perpendicular to each other. Two synchronized records of uptake at 4000 frames/s were obtained for most experiments. When two cameras were used, the average values for R_0 and uptake velocity were determined.

B. Image analysis

Experimental data were obtained from high-speed sequences as a function of time. Key measurements were the height of the meniscus within the tube h (see Fig. 1), the initial drop radius R_0, and the shape of the drop outside of the tube over time. The software TRACKER [40] was used to identify and follow the meniscus height through successive frames. The same software was used to fit a circle to the spherical cap profile of the drop prior to uptake [Fig. 2(b)]. R_0 is defined as the radius of this circle, and therefore the curvature of the drop (which determines Laplace pressure), but provides only an upper bound on the drop volume. To characterize the shape of the drop outside of the tube, two radii of curvature were

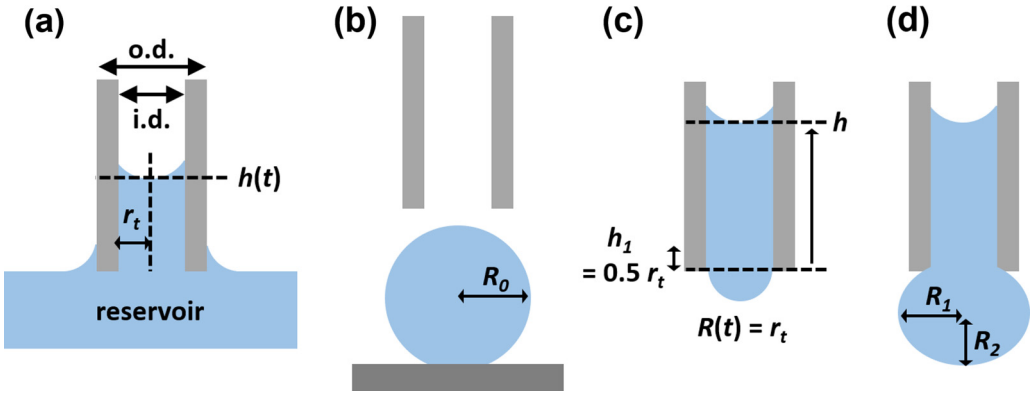

FIG. 1. Schematic diagrams of capillary uptake, showing key variables. (a) Uptake from a reservoir into a capillary of inner radius r_t, which fills to meniscus height $h(t)$. (b) A drop placed on a superhydrophobic surface (contact angle $\gtrsim$160°) has initial curvature R_0. (c) The drop comes into contact with the capillary. Height h_1 is discussed in the text. (d) The instantaneous Laplace pressure is calculated by measuring two curvatures (R_1 and R_2) for the (in general, nonspherical) drop outside the tube.

measured. Four positions were identified on the drop during uptake [Fig. 2(c)], and these were followed throughout the uptake sequence using TRACKER software. The measurement R_1 is defined as half the distance between points B and D, while R_2 is obtained by fitting a circle through points A, B, and C. The instantaneous Laplace pressure of the drop is then calculated as

$$\Delta P = \gamma\left(\frac{1}{R_1} + \frac{1}{R_2}\right). \tag{6}$$

A slightly different initial drop curvature ($R_0' = 2\gamma/\Delta P$) may be obtained using this method.

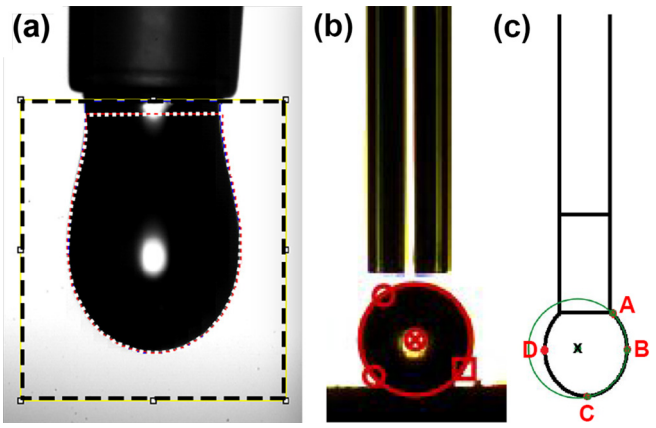

FIG. 2. Image analysis methods. (a) The outline of a pendant water drop hanging from a syringe tip is determined by an IMAGEJ plug-in [38] for measurement of surface tension. The user-defined dashed rectangular box defines the area in which the software identifies the outline (red and white dotted line). (b) A circular outline is fitted to a drop profile on a superhydrophobic surface prior to capillary uptake, using TRACKER software [40]. (c) Schematic diagram of a drop during capillary uptake, identifying the points used to calculate R_1 and R_2. Point A is where the drop meets the tube at the right edge, B and D define the maximum drop width, and C is the lowest point on the drop. The circular fit to points A, B, and C (thin line with the cross at its center) has radius R_2.

III. RESULTS AND DISCUSSION

A. Examples of meniscus rise

Figure 3 shows examples of $h(t)$ measurements for 0.75-mm borosilicate tubes in contact with drops of water and 10 wt % glycerol. In each case, experimental data are plotted for one of the very fastest moving menisci and one of the slowest. Each plot also includes lines corresponding to particular limiting velocities. The value of $v_{B,R}$ from Eq. (3), plotted for $R_0^{-1} = 0$, is a lower bound on purely inertial uptake. Equation (4) is used to plot $v_{f,R}$ for each experiment using the value $\chi_0 = 450$, as previously determined for uptake of water into glass [4]. When evaluating $v_{f,R}$, R is calculated as a function of time by assuming that the external drop is initially a sphere of radius R_0 and applying volume conservation. This approach provides an upper bound on the drop curvature. High-speed video sequences corresponding to the experiments in Fig. 3 are available in the Supplemental Material [16].

The results in Fig. 3 show that uptake speeds are always lower than $v_{B,R}$, as for previous measurements of uptake from reservoirs [1,4,20,25]. For aqueous solutions and glass, we expect $\cos\theta \approx 1$, so a mechanism such as contact line friction or a DCA must be important here. However, the speed of uptake typically exceeds $v_{f,R}$, even for some relatively slow moving menisci. These observations suggest that χ should be lower than Andrukh *et al.*'s value of $\chi_0 = 450$ [4]. Generally, uptake is faster for smaller drops, and this relationship is explored further in the next section.

Alignment of the drop with the capillary is variable. In these experiments, the center of the capillary was displaced horizontally by up to $\sim r_t$ from the center of the drop, and the angle of the tube was less than 5° (typically, 1° or 2°) from the vertical. However, misalignment did not have a clear systematic effect on uptake velocity. For example, the fastest-moving meniscus observed for uptake of water into a 0.75-mm borosilicate tube [Fig. 4(a)] has asymmetric alignment, resulting in an uneven meniscus at $t = 0$. The meniscus then quickly forms and penetrates into the capillary. In this case the momentum of the uptake is large enough that the entire volume enters the tube and forms a slug. This can be observed at $t = 27$ ms, which is when the upper meniscus

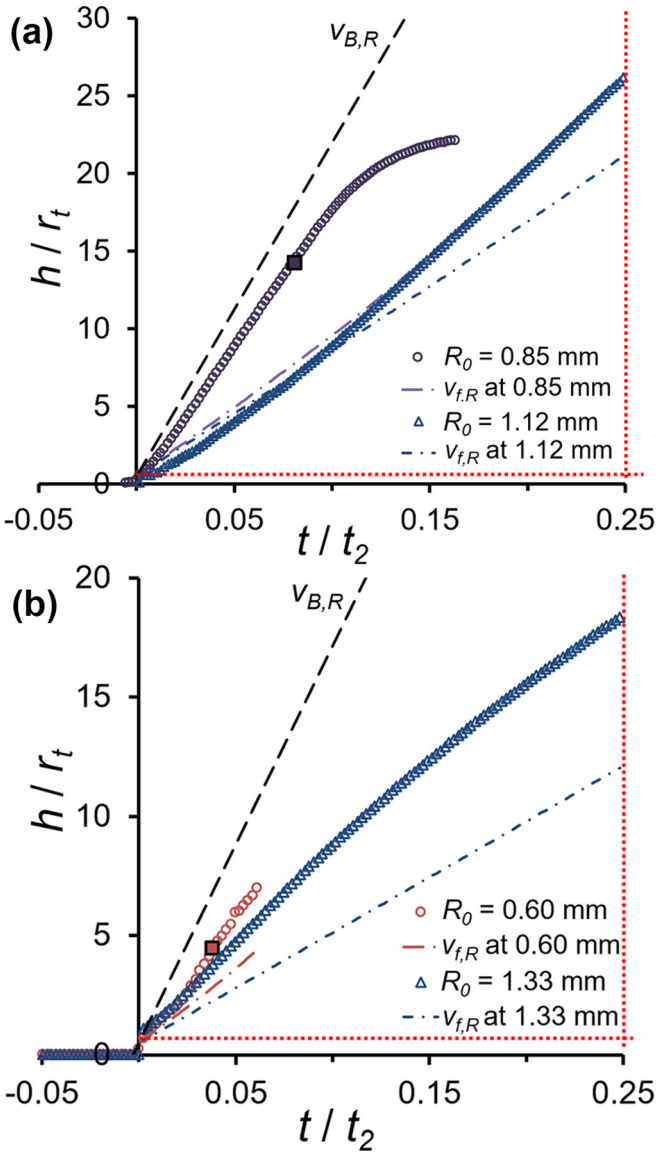

FIG. 3. Examples of measurements of meniscus position as a function of time for drop uptake into 0.75-mm borosilicate capillaries of (a) water and (b) 10% glycerol. Each plot includes data for one relatively small, fast drop and for one relatively large, slow drop, along with plots of $v_{B,R}$ (black dashed line) and $v_{f,R}$. All plots are shifted so that $t = 0$ when the meniscus reaches h_1. The outer red (gray) dotted lines indicate h_1 and $t_2/4$, and large square symbols indicate where uptake reaches h_2.

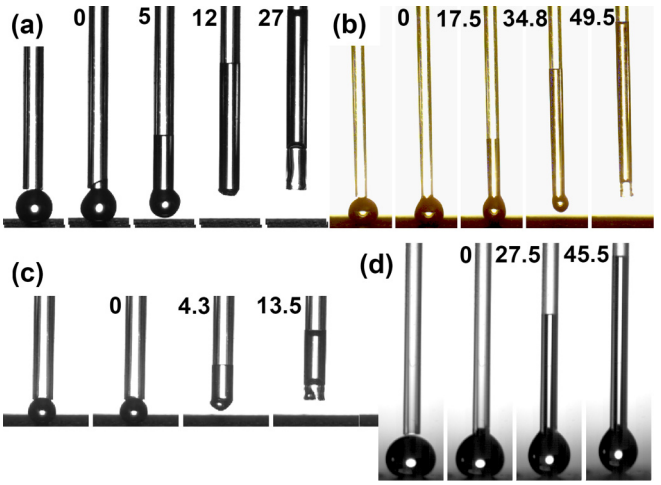

FIG. 4. Photographic sequences corresponding to experiments plotted in Fig. 3. The first frame in each sequence is prior to uptake, approximate times are labeled in milliseconds, and the original capture rate was 4000 frames/s. (a) Water, $R_0 = 0.85$ mm, (b) water, R_0=1.12 mm, (c) 10 wt % glycerol, $R_0 = 0.60$ mm, and (d) 10 wt % glycerol, $R_0 = 1.33$ mm.

stops advancing. In another example for a similar tube-liquid configuration [Fig. 4(b)], the drop is again slightly misaligned, but this time uptake is slow. The drop, which is larger than the fast-moving case, slightly oscillates from side to side following contact and after depinning from the surface. Pinning is apparent due to slight elongation of the drop at $t = 17.5$ ms. During this time, the h-t curve remains relatively smooth in Fig. 3(a).

For the more viscous 10 wt % glycerol solution, the velocities $v_{B,R}$ and $v_{f,R}$ are smaller due to increased liquid density. The example of a small, fast-moving drop [Fig. 4(c)] is initially well aligned with the capillary and forms a slug once uptake is complete. The larger drop in Fig. 4(d) is also reasonably well aligned with the tube and fills the tube smoothly but slowly once the meniscus is formed.

The electrostatically driven jump to contact recorded for previous experiments [3,19] was not clearly observed, although there were some examples of slight motion observed prior to contact (e.g., Supplemental Material Fig. S2 [16]). The Supplemental Material also contains further examples of uptake measurements and image sequences for smaller (0.50 mm) quartz and borosilicate capillary tubes and for 30 and 50 wt % glycerol solutions (Figs. S3–S5), as well as a demonstration that slower meniscus motion is systematically observed for as-received (as opposed to recently washed) capillaries (Fig. S6). Experiments in Figs. 3 and 4 were all carried out using recently cleaned capillaries.

The results in this section show that values of uptake velocity calculated using Eq. (3) are greater than experimental values, while calculations using Eq. (4) are typically smaller. In the next section, data are analyzed using Eq. (5), which includes both line friction and inertial contributions. The experimental velocity values have considerable variability, so it is appropriate to obtain mean values of χ using data from many experiments, rather than fitting Eq. (5) to individual experiments. It will also be important to establish that the data used lie within the inertial regime to check the assumption that the viscous contribution may be neglected.

B. Linear fits in the inertial regime

As described in the Introduction, an inertia-dominated uptake regime should follow establishment of the meniscus, and a systematic approach has been used to measure the velocity within this regime for our experiments. Solutions in the inertial regime become invalid once h is large, and viscous losses within the tube become significant. Transitions between capillary uptake regimes have been discussed

[2,25,30], notably by Fries and Dreyer [41], who identified the inertial-viscous transition with the characteristic viscous timescale, $t_2 = \rho r_t^2/\eta$. Transition times as high as $\sim 2.1 t_2$ [41] and as low as $t_2/16$ [2] have been suggested; in this paper we consistently use $t_2/4$, a relatively low value also used by Quéré [25]. The beginning of the inertial regime is also important because approaches such as Eq. (2) assume that a stable meniscus has been established within the capillary. An initial height of $h_1 = r_t/2$ has been suggested [2,25] and is consistent with recent experiments involving high-resolution observations of meniscus formation [4].

A constant meniscus velocity is expected in the inertial regime if the drop radius and contact angle are assumed to be constant, whether contact line friction is excluded [Eq. (3)] or not [Eq. (5)]. The slope of the h-t plot was initially determined for all experiments over the interval between the meniscus reaching h_1 and $t_2/4$. However, prior to $t_2/4$ the meniscus position often reaches a plateau where there is clearly a nonlinear h-t relation. This occurs when most of the drop's volume is inside the capillary tube. As a result, the interval for determining inertial velocity was truncated prior to $t_2/4$ if the volume of fluid outside of the tube was reduced to the volume of a hemisphere of radius r_t, which is approximately coincident with the onset of observed plateaus in Fig. 3. At this point, the curvature of a drop pinned at the entrance to the tube reaches a maximum, so the external Laplace pressure starts to decrease if further fluid enters the capillary. Using volume conservation, this occurs at a meniscus height of

$$h_2 = \frac{4}{3}\left(\frac{R_0^3}{r_t^2} - \frac{r_t}{2}\right). \tag{7}$$

Examples of the fitting interval are demonstrated in Fig. 3, where h_1 and $t_2/4$ are indicated by red dashed lines, and large square symbols are used to indicate where h_2 has been reached. The linear fit for the fast-moving water drop [Fig. 4(a)] is halted after $\sim$12 ms as the meniscus reaches h_2, whereas the fit for the experiment in Fig. 4(b) extends from t_0 to $t_2/4 = 34.8$ ms, at which point the drop is nearly completely within the capillary. For 10 wt % glycerol drops, t_2 is reduced, and the fast-moving case [Fig. 4(c)] reaches h_2 after just 4.3 ms, prior to forming a slug. Identification of h_2 has some uncertainty because R_0 is used to calculate the initial volume (giving an upper bound) and because the external meniscus may not be pinned at the internal diameter of the tube.

Table II includes summary statistics for linear fits to the h-t data over the specified inertial range for the experiments analyzed. Linear fits to the data are generally appropriate, as indicated by the mean coefficient of determination values R^2 close to 1. The $v_{f,R}$ plots in Fig. 3 also indicate that changing drop curvature is not expected to produce large deviations from a linear h-t trend. Relatively low R^2 values were usually recorded when a small number of data points were sampled. This is particularly the case for smaller drops, which have relatively low values of h_2 and fast meniscus velocities.

Figure 5 shows inertial regime velocity data for experiments in which the measured velocity exceeded the value of $v_{f,R}$ calculated for $R_0^{-1} = 0$. Experiments producing velocities below this value were often those using as-received capillaries

TABLE II. Summary of linear h-t fits to experimental results in the inertial regime, where n is the number of experiments in each case. Experiments used 0.75-mm borosilicate tubes unless otherwise stated.

Solution	n	R^2 (Mean)	χ (± 1)
Water	44	0.99	218
0.50 mm	77	0.99	217
0.50 mm, quartz	55	0.99	197
Glycerol			
10 wt %	28	0.99	216
30 wt %	57	0.99	215
50 wt %	59	0.96	169

(Supplemental Material Fig. S6 [16]). As observed previously [3], uptake velocity generally increases with drop curvature due to the droplet Laplace pressure. A comparison with uptake from reservoirs is provided by the experiments for water and borosilicate tubes at $R_0^{-1} = 0$ mm, and the predicted influence of Laplace pressure (see the differences in the $v_{B,R}$ values listed in Table I) is broadly consistent with the observations.

As was the case for the examples shown in Fig. 3, the population data also have meniscus speeds considerably lower than the value of $v_{B,R}$ calculated at $R_0^{-1} = 0$, let alone higher values driven by drop curvature. Importantly, the experimental dependence of uptake velocity on R_0 is not clearly monotonic. In the Introduction, various explanations for velocities smaller than a purely inertial value were described. Of these, stochastic variation is expected only if friction plays a role, as this mechanism is affected by imperfections in the capillary surface which give rise to contact line pinning. Contact line friction is also consistent with the large observed decrease in uptake velocity with increasing drop viscosity. In Supplemental Material Fig. S7 [16], uptake velocities decrease with viscosity when they are normalized using v_B, demonstrating

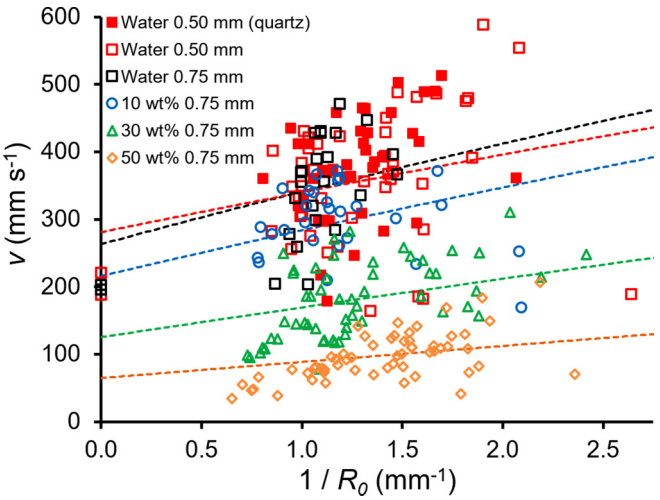

FIG. 5. Measured velocities in the inertial regime for all experiments exceeding the value of $v_{f,R}$ calculated for $R_0^{-1} = 0$. Lines indicate values of $v_{B,f,R}$ with least-squares fits of the parameter χ for the data series of the same color (borosilicate only). $R_0^{-1} = 0$ mm^{-1} corresponds to a reservoir.

that the trend cannot be directly explained by variations in fluid density or tube radius. A small decrease in inertial velocity $v_{B,R}$ is expected due to changes in surface tension for the glycerol solutions relative to water (Table I). The experimentally observed changes are much larger, confirming the presence of a material-dependent mechanism other than inertia.

Assuming that the inertial dynamics are affected by contact line friction, we can find least-squares fits to $v_{B,f,R}$ [Eq. (5)] using the coefficient χ as a variable. This is appropriate because, as noted above, the value $\chi_0 = 450$ predicts values of $v_{f,R}$ [Eq. (4)] that are lower than those observed. Also note that Eq. (5) includes inertial effects, whereas χ_0 was used with Eq. (4) in Ref. [4]. Fits to the data plotted in Fig. 5 give the corresponding mean values of χ listed in Table II. These means are identified with a precision of ± 1, and based on calculated velocities, each fit gives a standard error of the mean of $<6\%$. These values confirm that the value of $\chi_0 = 450$ for water is higher than suggested by our data. These values are calculated using the assumption that $\cos\theta = 1$, and here, we note that it is possible to recast contact line friction as a DCA [32], taking the form $\theta_D = 1 - (\eta\chi/\gamma)(dh/dt)$ when $\cos\theta \approx 1$. Here, it seems that unrealistic contact angle values ($\theta_D \gtrsim 45^\circ$) would be required for agreement with experimental data.

As long as washed capillaries are used, there is no clear difference in the water uptake velocities when the tube diameter and material are varied. It is usually expected [4] that uptake velocity would be faster in a smaller tube in the inertial regime [$v_B \propto 1/r_t$, Eq. (3)], whereas the opposite is true for friction-dominated dynamics [$v_{f,R}$ increases with r_t/R, Eq. (4)] and Lucas-Washburn dynamics ($v \propto r_t^{\frac{1}{2}}$). The apparent competition between these trends is consistent with the interpretation that both inertia and viscosity-dependent contact line friction are playing a significant role in determining the uptake speed.

Overall, Eq. (5) provides a good description of the experimental data and explains the observations of stochastic variation. More complex models could be developed for drop uptake by including second-order contributions. These include terms from Eq. (1) proportional to h and d^2h/dt^2, along with viscosity and gravity. Variability in the values of c, s, and κ [2] could be considered, and the analysis of drop curvature external to the capillary could be developed.

Other effects may be particularly relevant to applications outside the laboratory. For example, there are many ways in which the liquid outside of the capillary can affect uptake. Practical examples include moving liquid surfaces [19], the importance of the position of the contact line [24] and the external (outer wall) meniscus [4], and drops which cover multiple pores [7]. Also, there can be variations in the way in which the tube and the drop come into contact, and the importance of initial conditions has been noted in previous studies [1,4,42], although a description of uptake which includes these is still largely lacking. It is reasonable to suggest that although misalignment did not have a clear systematic effect for the examples in Fig. 4, the exact alignment could contribute to variation in uptake dynamics in a way not captured by the analytical models used here. In those models, the drop is centrally aligned with the tube, and the tube's outer diameter is not considered, although here the experimental geometry

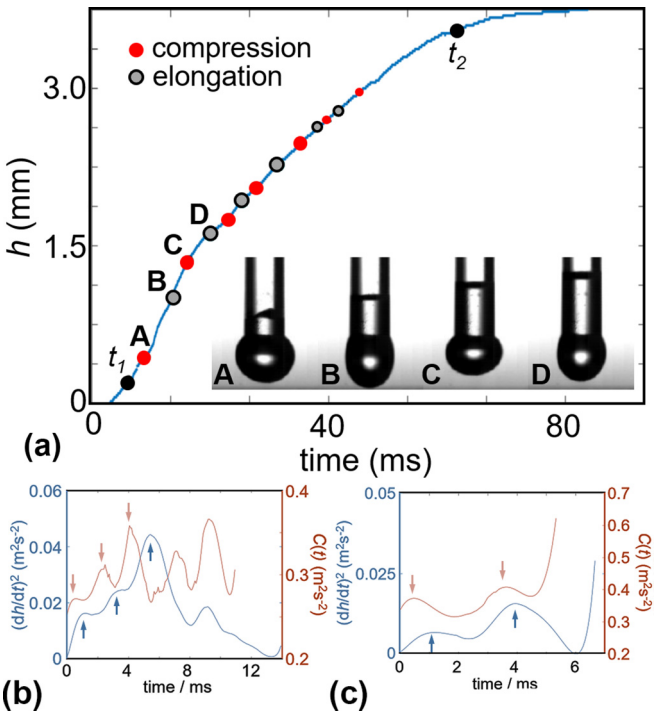

FIG. 6. (a) Meniscus height rise for a water drop ($R_0^{-1} = 0.95\ \mathrm{mm}^{-1}$) entering a 0.75-mm borosilicate capillary. Times corresponding to compression and elongation of the external drop are identified, and images for the first four of these times are inset and labeled A–D. (b) Comparison of the square of the velocity (blue lower line) with instantaneous Laplace pressure (red upper line) for uptake of water with $R_0'^{-1} = 1.21\ \mathrm{mm}^{-1}$ into a 0.75-mm borosilicate tube and (c) a similar comparison for 10% glycerol with $R_0'^{-1} = 1.75\ \mathrm{mm}^{-1}$ into a 0.75-mm borosilicate tube. Arrows indicate local peak positions for the first few peaks in each series.

does not encourage an external meniscus as observed for reservoir uptake [4]. In addition, capillary waves are observed in the experiments when a drop contacts the tube, or depins from the surface. The influence of these waves on uptake velocity, including an apparent link between the dynamics of the external drop and the uptake speed observed, is considered in the following section.

C. Time-resolved Laplace pressure

Capillary waves are generated when a drop comes into contact with the tube or depins from the surface on which it initially rests. This is the main cause of the aspherical and asymmetric drop shapes observed during uptake, as in Fig. 4. For a further example shown in Fig. 6(a), $h(t)$ has been measured, and the times corresponding to maximum compression and elongation of the oscillating external drop have been identified. In this case, the data extend beyond the limits of the inertial regime used above (h_2 or $t_2/4$), and the uptake velocity is clearly no longer constant. The oscillations identified here differ from those reported for similar experiments [1,25] which occurred when the uptake process was essentially complete.

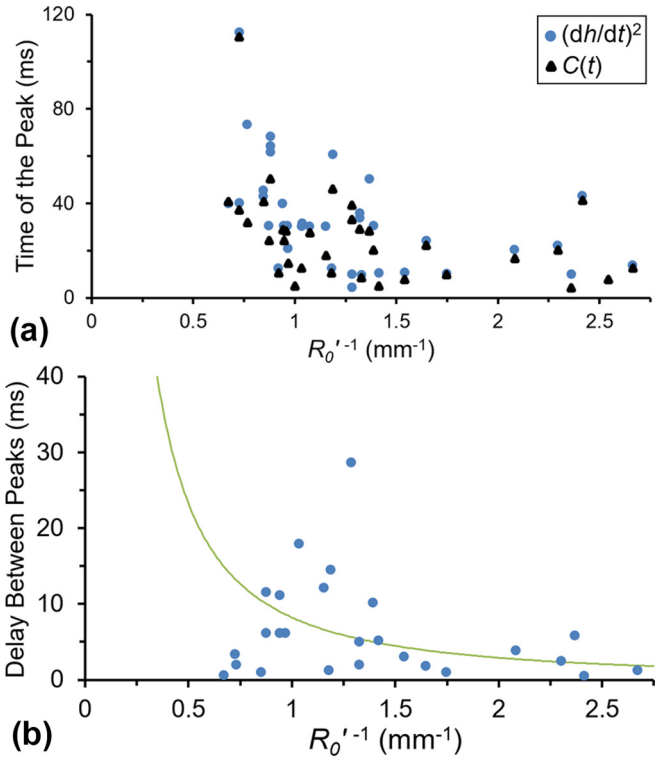

FIG. 7. (a) The first peaks appearing in traces for uptake of water drops into 0.75-mm borosilicate tubes. (b) The time delay between the first pressure peak and the first velocity peak for each of these experiments. The line indicates the inertial-capillary timescale [Eq. (8)].

Figure 6(a) and similar experiments qualitatively suggest a correlation between the oscillations and the meniscus velocity. To further study the effect of the instantaneous Laplace pressure on measurements of $h(t)$, R_1 and R_2 have been tracked over time as described in Sec. II. A variable C is defined to represent the instantaneous Laplace pressure, so that $\rho C = \Delta P$, where ΔP is defined in Eq. (6). Qualitatively, it is expected that $(dh/dt)^2$ should increase when C increases [see Eq. (2), for example].

Figures 6(b) and 6(c) are examples of results which show an apparent link between peaks in the velocity and Laplace pressure. There is a notable lag between the local peak positions in Figs. 6(b) and 6(c), particularly for the first two or three peaks (see arrows), with the Laplace pressure reaching a maximum shortly before the velocity. To determine the reproducibility of this observation, the timing of the first peak was studied over many experiments, with peaks identified using a threshold of half a standard deviation from the mean value over a moving window of 10-ms duration.

Data for water drops and 0.75-mm borosilicate tubes in Fig. 7(a) confirm that the first pressure peak almost always precedes the first velocity peak. The data are generally consistent across smaller drops ($R_0'^{-1} > 1.5$ mm^{-1}), whereas for larger drops the oscillations were more variable, and delays prior to the first oscillation were often longer. For larger drops, oscillations associated with depinning from the surface could be significant.

The range of time delays between the first pressure peak and the first velocity peak is shown in Fig. 7(b). Similar data are presented in the Supplemental Material (Fig. S8) for water interacting with 0.50-mm borosilicate and quartz tubes and for uptake of 30 wt % glycerol drops into 0.75-mm borosilicate tubes [16]. The timescale for this delay is comparable to the inertial-capillary oscillation time plotted in these figures, which describes the lowest-order oscillatory period of a spherical drop [43,44],

$$\tau = \pi\sqrt{\frac{\rho R^3}{2\gamma}}. \tag{8}$$

Inertial-capillary oscillations provide an explanation for the delay, although the measurements vary both above and below the inertial-capillary time, especially at low values of $R_0'^{-1}$. It is postulated that this variability is associated with the specific geometries for particular drops and oscillations. When there are relatively long delays, contact line pinning is probably playing a role. When the three phase line is pinned, the contact angle must increase prior to motion of the meniscus, and this meniscus rearrangement can cause the observed lag. Vejrazka *et al.* [45] studied the eigenmodes for oscillations of a drop on the end of a capillary, and it may be possible to use such an analysis to more closely link the drop motion with uptake velocity. Note that the measured delay times are inconsistent with the speed of pressure (sound) waves, which would traverse a millimetric water drop in 10^{-6} or 10^{-7} s.

IV. CONCLUSIONS

Experimental results from this study have provided a quantitative description of liquid drop uptake into capillary tubes. The rate of uptake is predominantly linear within the inertial regime, as predicted using an extension to existing descriptions of reservoir uptake. The limits of the inertial regime were defined conservatively, and during these intervals the drop radii changed significantly, but data obtained after the drop outside of the tube formed a hemisphere were excluded. The influence of Laplace pressure was observed due to the increase of inertial velocities with drop curvature, and velocities for washed tubes were predominantly lower than the inertia-dominated velocity $v_{B,R}$ but higher than the friction-dominated velocity $v_{f,R}$. A model which incorporates both inertia and contact line friction has been used to explain the observed dynamics due to apparently stochastic variations in the measured velocity (consistent with a stick-slip mechanism) and the increasing role of friction with fluid viscosity. Derived values of the mean contact line friction coefficient for water on glass were considerably lower than a previously reported value [4].

For applications such as microfluidic drop manipulations and understanding of drop uptake by microporous materials, detailed understanding or close reproducibility of the uptake dynamics may become important. As a step towards understanding the importance of variation in the external drop shape, drop oscillations were measured to obtain an instantaneous Laplace pressure. When uptake starts, the typical delay between the first peak in this pressure and the following velocity peak is similar in magnitude to the timescale for inertial-capillary oscillations.

[1] K. G. Kornev and A. V. Neimark, J. Colloid Interface Sci. **235**, 101 (2001).
[2] M. Stange, M. E. Dreyer, and H. J. Rath, Phys. Fluids **15**, 2587 (2003).
[3] G. R. Willmott, C. Neto, and S. C. Hendy, Soft Matter **7**, 2357 (2011).
[4] T. Andrukh, D. Monaenkova, B. Rubin, W. K. Leec, and K. G. Kornev, Soft Matter **10**, 609 (2014).
[5] M. O'Loughlin, K. Wilk, C. Priest, J. Ralston, and M. N. Popescu, J. Colloid Interface Sci. **411**, 257 (2013).
[6] A. Marmur, J. Colloid Interface Sci. **122**, 209 (1988).
[7] H. Choi and H. Liang, J. Colloid Interface Sci. **477**, 176 (2016).
[8] D. Schebarchov and S. C. Hendy, Nano Lett. **8**, 2253 (2008).
[9] D. Schebarchov and S. C. Hendy, Phys. Rev. E **78**, 046309 (2008).
[10] Z. Wang, H. Y. Yen, C. C. Chang, Y. J. Sheng, and H. K. Tsao, Langmuir **29**, 12154 (2013).
[11] K. G. Kornev and A. V. Neimark, J. Colloid Interface Sci. **262**, 253 (2003).
[12] S. Levine, P. Reed, E. J. Watson, and G. Neale, in *Colloid and Interface Science*, edited by M. Kerker (Academic, New York, 1976), Vol. 3, pp. 403–419.
[13] P. R. Waghmare and S. K. Mitra, J. Fluids Eng. **132**, 054502 (2010).
[14] A. Marmur, J. Colloid Interface Sci. **123**, 161 (1988).
[15] A. V. Bazilevsky, K. G. Kornev, A. N. Rozhkov, and A. V. Neimark, J. Colloid Interface Sci. **262**, 16 (2003).
[16] See Supplemental Material at http://link.aps.org/supplemental/10.1103/PhysRevE.101.043109 for capillary uptake videos, further image sequences, and further uptake velocity and peak delay data.
[17] R. Lucas, Kolloid-Z. **23**, 15 (1918).
[18] E. W. Washburn, Phys. Rev. **17**, 273 (1921).
[19] G. R. Willmott, C. Neto, and S. C. Hendy, Faraday Discuss. **146**, 233 (2010).
[20] S. Palzer, K. Sommer, and C. Hiebl, Chem. Eng. Technol. **26**, 962 (2003).
[21] M. Radiom, W. K. Chan, and C. Yang, Microfluid. Nanofluid. **7**, 697 (2009).
[22] A. Delbos, E. Lorenceau, and O. Pitois, J. Colloid Interface Sci. **341**, 171 (2010).
[23] Y. Wang, S. Chen, and B. Wu, Comput. Fluids **154**, 211 (2017).
[24] P. Yue and Y. Renardy, Phys. Fluids **25**, 052104 (2013).
[25] D. Quéré, Europhys. Lett. **39**, 533 (1997).
[26] C. L. Trabi, F. F. Ouali, G. McHale, H. Javed, R. H. Morris, and M. I. Newton, Langmuir **32**, 1289 (2016).
[27] N. K. Karna, E. Oyarzua, J. H. Walther, and H. A. Zambrano, Phys. Chem. Chem. Phys. **18**, 31997 (2016).
[28] O. Shardt, P. R. Waghmare, J. J. Derksen, and S. K. Mitra, RSC Adv. **4**, 14781 (2014).
[29] C. J. Ridgway, P. A. C. Gane, and J. Schoelkopf, J. Colloid Interface Sci. **252**, 373 (2002).
[30] A. Siebold, M. Nardin, J. Schultz, A. Walliser, and M. Oppliger, Colloids Surf. A **161**, 81 (2000).
[31] H. T. Xue, Z. N. Fang, Y. Yang, J. P. Huang, and L. W. Zhou, Chem. Phys. Lett. **432**, 326 (2006).
[32] A. Hamraoui, K. Thuresson, T. Nylander, and V. Yaminsky, J. Colloid Interface Sci. **226**, 199 (2000).
[33] M. N. Popescu, J. Ralston, and R. Sedev, Langmuir **24**, 12710 (2008).
[34] P. Wu, A. D. Nikolov, and D. T. Wasan, Langmuir **33**, 7862 (2017).
[35] D. Quéré, Annu. Rev. Mater. Res. **38**, 71 (2008).
[36] A. Volk and C. J. Kähler, Exp. Fluids **59**, 75 (2018).
[37] W. M. Haynes, *CRC Handbook of Chemistry and Physics* (CRC Press, Boca Raton, FL, 2015).
[38] A. Daerr and A. Mogne, J. Open Res. Software **4**, e3 (2016).
[39] I. A. Larmour, S. E. J. Bell, and G. C. Saunders, Angew. Chem., Int. Ed. **46**, 1710 (2007).
[40] D. Brown, Computer program tracker video analysis and modeling tool, Version 4.96 (2017), http://physlets.org/tracker/.
[41] N. Fries and M. Dreyer, J. Colloid Interface Sci. **327**, 125 (2008).
[42] E. Oyarzua, J. H. Walther, A. Mejía, and H. J. Zambrano, Phys. Chem. Chem. Phys. **17**, 14731 (2015).
[43] J. C. Bird, R. Dhiman, H.-M. Kwon, and K. K. Varanasi, Nature (London) **503**, 385 (2013).
[44] H. Lamb, *Hydrodynamics* (Cambridge University Press, Cambridge, 1895), pp. 461–463.
[45] J. Vejrazka, L. Vobecka, S. Orvalho, M. Zednikova, and J. Tihon, Chem. Eng. Sci. **116**, 359 (2014).